Automatic Lumbar Vertebra Segmentation from clinical CT for Wedge Compression Fracture Diagnosis

Subarna Ghosh[a], Raja' S. Alomari[a], Vipin Chaudhary[a], Gurmeet Dhillon[b]
{sghosh7, ralomari, vipin}@buffalo.edu {gdhillon}@proscan.com
[a]University at Buffalo, SUNY, Buffalo, NY 14260
[b]ProScan Imaging of Buffalo, Williamsville, NY 14221

ABSTRACT

Lumbar vertebral fractures vary greatly in types and causes and usually result from severe trauma or pathological conditions such as osteoporosis. Lumbar wedge compression fractures are amongst the most common ones where the vertebra is severely compressed forming a wedge shape and causing pain and pressure on the nerve roots and the spine. Since vertebral segmentation is the first step in any automated diagnosis task, we present a fully automated method for robustly localizing and segmenting the vertebrae for preparation of vertebral fracture diagnosis. Our segmentation method consists of five main steps towards the CAD(Computer-Aided Diagnosis) system: 1) Localization of the intervertebral discs. 2) Localization of the vertebral skeleton. 3) Segmentation of the individual vertebra. 4) Detection of the vertebrae center line and 5) Detection of the vertebrae major boundary points. Our segmentation results are promising with an average error of $1.5mm$ (modified Hausdorff distance metric) on 50 clinical CT cases *i.e.* a total of 250 lumbar vertebrae. We also present promising preliminary results for automatic wedge compression fracture diagnosis on 15 cases, 7 of which have one or more vertebral compression fracture, and obtain an accuracy of 97.33%.

Keywords: Lumbar Spine, Wedge Compression Fracture, Computer Aided Diagnosis, CT, lumbar vertebra segmentation.

1. INTRODUCTION

Lower back pain (LBP) is the second most common neurological ailment in the United States after headache[1] with $50 billion spent annually on rehabilitation and health care of LBP. Vertebral and intervertebral disc abnormalities are the major causes of LBP. Hence, lumbar area research mainly focuses on the automation (and semi-automation) of disc and vertebral abnormality detection. Localization and segmentation of the vertebrae and the intervertebral discs are usually the first steps for most diagnosis tasks. Currently various imaging modalities are used in clinical settings for scanning the lower spine depending on the severity of pain, availability of scanners, cost and total time required for the acquisition. X-ray radiography and DXA(Dual-emission X-ray absorptiometry) are usually the cheapest and are taken as an initial step for diagnosis. CT and/or MRI, due to their substantially higher cost and better diagnostic value comes next. While CT is the preferred modality for trauma patients, MRI (which is more expensive than CT and has a higher acquisition time) is used more often for pathological conditions.

Wedge fractures are the most common type of lumbar fracture and are the typical compression fracture of malignancy or osteoporosis.[2] They occur as a result of an axially directed central compressive force combined with an eccentric compressive force as shown in Fig. 1. Although wedge fractures are usually symmetric, 8-14% are asymmetric and are termed as lateral wedge fractures.

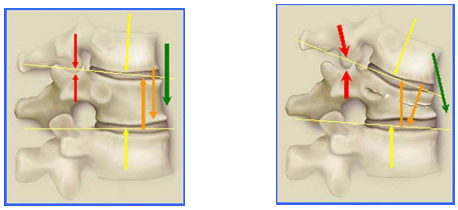

(a) Normal (b) Wedge Fracture.

Figure 1: Anterior Wedge Compression Fracture

The symptoms of a compression fracture are sudden back pain, often with radiculopathic pain (shooting pain due to nerve root compression). Multiple vertebral fractures lead to a stooped posture, loss of height, and chronic pain with resultant reduction in mobility.[3]

Fractures in the lumbar spine occur for a number of reasons. In younger patients, fractures are usually due to violent trauma like car and sport related accidents. In older patients, lumbar compression fractures usually occur in the absence of trauma, or in the context of minor trauma, such as a fall. The most common underlying reason for these fractures in geriatric patients, especially women, is osteoporosis.[4] Malignancy, infections, and renal disease can also contribute to the occurrence of compression fractures. Lumbar compression fracture can be a devastating injury not only because it can cause significant pain, but also because it can alter the mechanics of the posture to the point that the patient cannot stand upright. Hence rapid diagnosis of compression fracture is extremely important for immediate orthopedic attention.

2. PREVIOUS WORK

Although discs and vertebra in CT and MRI images are prominent and have well-defined boundaries from a human observer's point of view; labeling and segmentation is challenging for a fully automated algorithm since the CT and MRI images can be extremely inhomogeneous, neighboring irrelevant structures can be connected and might have similar intensities. Recent research on spine has been focusing on vertebral and disc localization and segmentation from various medical modalities including X-rays and DXA,[5] CT[6] and MRI.[7,8] The purpose of the segmentation is to provide robust and automated tools for further diagnosis tasks such as our previous work.[9–11]

Probabilistic graphical models have been used for spine localization and labeling such as Schmidt et al.[7] whose work focuses on the whole spine and Alomari et al.[8] focusing only on lumbar area. Their models incorporated both appearance and space information of the discs to localize and label the discs from MRI. Schmidt et al.[7] presents a probabilistic graphical model for representing both the appearance of local parts and the shape of the anatomy in terms of geometric relations between parts. Intially, features for detecting parts are learned from a set of training data in manually marked image regions, then, in the detection stage, a multi-class classifier is applied to detect potential locations for each part in a new image. Finally, the graphical model provides a contextual decision by fusing these data with the geometrical prior knowledge and infers the globally optimal configuration of the parts. Alomari et al.[8] proposes a two-level probabilistic model for the localization of discs from lumbar clinical MRI data that captures both pixel- and object-level features. Using a Gibbs distribution, they model appearance and spatial information at the pixel level, and at the object level, they model the spatial distribution of the discs and the relative distances between them. They use generalized expectation-maximization for optimization, which achieves efficient convergence of disc labels.

Roberts et al.[5] present a fully automatic method of segmenting vertebrae in spinal radiographs using parts-based graphs and Active Appearance Models, but have a high failure rate for fractured vertebrae. Research using CT volumes for interactive and fully-automatic vertebra segmentation are also investigated in the literature.[12,13] However, they work poorly for defective and fractured vertebra, and cases with disc disorders. Naegel et al.[13] describes a method for the labeling and segmentation of vertebrae in CT scans based on the computation of the separation planes of the vertebrae and mathematical morphology operators using anatomical assumptions. In order to detect the intervertebral spaces, they use a morphological operator which detects the dark spaces corresponding to intervertebral discs in combination with an analysis of the shape of the vertebrae in the axial plane. To reconstruct the vertebrae they find internal and external markers and then perform watershed segmentation. Finally, to label the vertebrae, they deduce the T12 vertebrae by marking all the vertebrae connected to the ribs and keeping the lowest one. Kaminsky et al.[12] presents a fast 3D visualization and segmentation system that uses two special interactive tools and a standardized protocol for segmentation adapted to the needs for segmentation procedures of spine segments. It consists of both automated and interactive steps and is also applicable to instrumented and severely degenerated regions of the spine, although, additional interactive steps were necessary making the process very slow.

Precise segmentation of lumbar vertebrae in CT images was proposed by Mastmeyer et al. [6] They developed a hierarchical 3D technique to segment the vertebral bodies in order to measure bone mineral density(BMD) with high trueness and precision in volumetric CT datasets of the lumbar spine. However, initial landmarks had to be manually placed in the vertebral bodies. For thoracic CT volumes Shen et al.[14] recently presented an automatic vertebra segmentation algorithm where vertebra labeling was not addressed. They proposed a prior knowledge base that contains localized priors - a group of high-level features whose detection augments their

surface model. They validated their algorithm on 21 CT volumes, but do not specify the presence or absence of vertebral abnormalities or fractures. Klinder et al.[15] proposed statistical surface models for each of the vertebra and the sacrum. They automate the detection of vertebra from unspecified spinal regions by using generalized Hough transform models, but are highly dependent on the training data.

In this paper, we only focus on clinical lumbar CT scans. In everyday clinical routine, radiologists order separate spinal areas for CT and MRI due to both cost and acquisition time-related issues. We propose an automatic and accurate method for segmentation of each vertebra and prepare it for feature extraction and wedge compression fracture diagnosis.

3. PROPOSED METHOD AND DATA

Our data consists of 50 anonymized clinical CT volumes. These cases contain various types of fractures, bone spurs, and several disc abnormalities. We also obtain the clinical diagnosis report along with each case from which we obtain our gold standard for the diagnosis. The following steps summarize our proposed method.

3.1 Discs localization

We utilize our previous work[8] for this step as this method proves its robustness on clinical data. This method provides a point inside each disc from Lumbar MRI images. We applied the method on lumbar clinical CT and found its high accuracy that made it the best choice for this step. This method presents a two-level probabilistic model that labels the set of discs with high level labels $\mathtt{D} = \{d_1, d_2, \ldots, d_6\}$ where each $d_i = (x_i, y_i)^\mathsf{T}$ is the coordinates of the disc point (some point in the disc). Then the following optimization problem is solved using a generalized expectation maximization (GEM) algorithm:[8]

$$\mathtt{D}^* = \arg\max_{\mathtt{D}} \sum_{\mathtt{L}} P(\mathtt{L}, \mathtt{D}|\mathtt{I}) = \arg\max_{\mathtt{D}} \sum_{\mathtt{L}} P(\mathtt{L}|\mathtt{D}, \mathtt{I}) P(\mathtt{D}) \tag{1}$$

where $\mathtt{L} = \{l_i,\ \forall i \in \mathtt{L}\}$ is a set of auxiliary variables, called disc-label variables that are introduced to infer $\mathtt{D}$ from the sagittal image. Each disc-label variable can take a value of $\{-1, +1\}$ for non-disc or disc, respectively. The disc-labels make it plausible to separate the disc variables from the image intensities, *i.e.*, the disc-label $\mathtt{L}$ variables capture the local pixel-level intensity models while the disc variables $\mathtt{D}$ capture the high-level geometric and contextual models of the full set of discs.

3.2 Vertebral skeleton localization

We start this step from the middle sagittal slice of the CT volume as shown in Fig. 2(a) where we convert it into the Hounsfield scale and clamp the image between 0 and 1000. This is based on the fact that bone is usually around 400 HU and higher.[16] We then segment the vertebral skeleton, *i.e.* the vertebral column region, by morphological operations including an opening-closing by reconstruction and subsequently dilating the threshholded image which gives us a rough ROI(Region of Interest) as shown in Fig. 2(b).

3.3 Individual Vertebra segmentation

After the first two steps, we segment each vertebra as shown in Fig. 2(d). We base this step on two main aspects: 1) Intensity and 2) Geometry. The intensity is represented by calculating the Gradient Image as:

$$G[\mathtt{I}] = \sqrt{(G_x^2 + G_y^2)} \tag{2}$$

where I is the image obtained after the vertebral skeleton localization, (x, y) represents the image pixel coordinates, G_x and G_y are the image gradients in the x and y direction respectively. This gradient image is used to detect Hough lines representing the horizontal edges of the lumbar vertebrae at each disc level as shown by the green lines in 2(c). These lines result from the Hough Transform which is parameterized as:

$$\rho = x\cos\theta + y\sin\theta \tag{3}$$

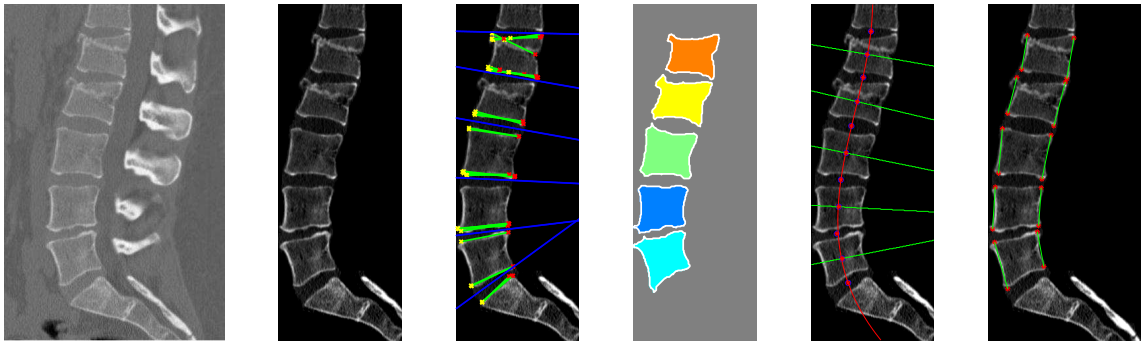

(a) (b) (c) (d) (e) (f)

Figure 2: Fully automated processing steps for a case with vertebral fracture at L1 and L2: (a) shows the original CT scan, (b) shows the extracted ROI, (c) shows the Hough Lines in green and the vertebra separating lines in blue, (d) shows the segmented and labelled vetebrae, (e) shows the vertebral centerline in red and orientation of each vertebra in green, (f) shows the automatically detected vertebral corners in red and the left and right vertebra height in green.

where θ is the angle of the vector from the origin to the line and ρ is distance between the line and the origin. Thus at each disc level, we calculate the mean Hough line slope as m_i where $1 \leq i \leq 6$.

Subsequently, geometry uses the set of points D resulting from Eq. 1 to find straight lines crossing the intervertebral discs at a suitable angle to separate two adjacent vertebrae as shown in Fig. 2(c) by the blue lines. These lines result from the line equation $y = mx + c$ where m is the slope and c is the y-intercept of the line. To compute each line, we use the point inside the disc d_i (detailed in subsection 3.1) and the slope m_i which is the mean slope of the Hough lines as generated in the previous step. Thus, we extract angle-constrained Hough lines from the gradient image G which gives us information about the inclination of line segments that separate two adjacent vertebrae.

After we obtain the rough horizontally segmented vertebrae, we perform image processing operations on each of the five lumbar vertebral regions to obtain smooth contours. First we convert the gray-scale image to black and white, then perform a hole filling operation followed by a morphological opening to remove tiny blobs. Then we retain the largest blob in that specific vertebral region and perform closing and hole filling operations to get a smooth vertebra boundary as shown in 2(d).

3.4 Vertebrae center line

This step aims at preparation of the vertebrae to extract features for the automatic diagnosis of compression wedge fracture. Using the disc center points D (from Eq. 1), we compute a third-degree polynomial to fit the lumbar curvature. The red curve in Fig. 2(e) shows a sample. We only concentrate on the lumbar area where the center line smoothly crosses the centers of the vertebrae. The accurate computation of the centerline allows accurate calculation of the normals that crosses each vertebrae as shown in Fig. 2(e) in green lines.

3.5 Vertebrae major boundary points

In this step, we compute eight boundary points for each vertebra that represent four corners and four mid-way points for the four edges. Calculation of these points is completely based on geometry operators using the disc localization points D, the lines crossing the discs, the smooth vertebral centerline and the normals within each vertebra. The computation of these points presents us with various features for designing suitable classifiers for the wedge fracture diagnosis as well as various vertebral abnormalities.

Figure 3 shows the automated processing steps of a case with no vertebral fracture while Figure 2 shows similar steps for a case with fractures at the L1 and L2 vertebrae.

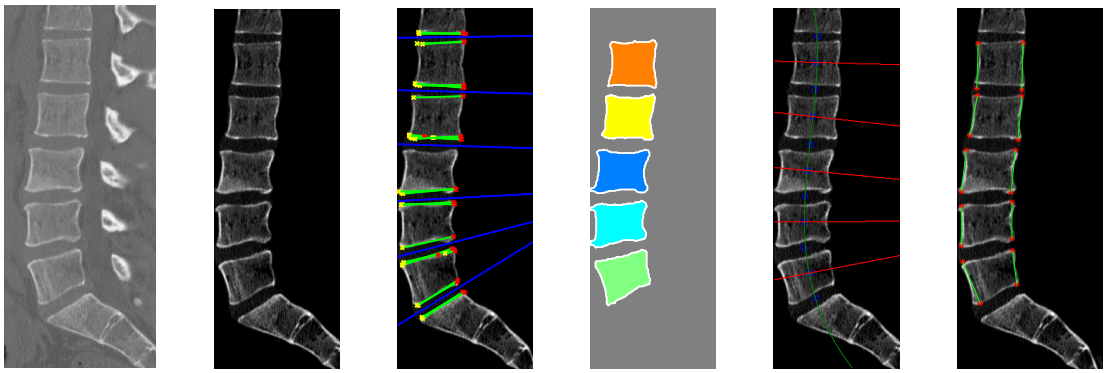

(a) (b) (c) (d) (e) (f)

Figure 3: Fully automated processing steps for a case with no vertebral fracture : (a) shows the original CT scan, (b) shows the extracted ROI, (c) shows the Hough Lines in green and the vertebra separating lines in blue, (d) shows the segmented and labelled vetebrae, (e) shows the vertebral centerline in blue and orientation of each vertebra in red, (f) shows the automatically detected vertebral corners in red and the left and right vertebra height in green.

3.6 Classification

After extracting the vertebrae major boundary points, we compute the left height $H_l(i)$, center height $H_c(i)$ and right height $H_r(i)$ of the ith vertebra of each case where $1 \leq i \leq 5$ (five lumbar vertebrae) as shown in Figures 2(f) and 3(f). This helps us extract a series of height features for each vertebra for automatic detection of wedge/compression fracture as discussed below.

3.6.1 Vertebra Height Features

We calculate three height ratio features as $H_l(i)/H_r(i)$, $H_l(i)/H_c(i)$, $H_r(i)/H_c(i)$ for each vertebra. These are important since for wedge/compression fractures, the relative left, right and center heights of a vertebra are very different from a vertebra with no fracture. We also calculate three height deviation features $Dev_l(i)$, $Dev_c(i)$, $Dev_r(i)$ for the ith vetebra defined as :

$$Dev_l(i) = max(H_l) - H_l(i) \quad ; \quad Dev_c(i) = max(H_c) - H_c(i) \quad ; \quad Dev_r(i) = max(H_r) - H_r(i) \tag{4}$$

where $max(H_l)$ is the maximum left vertebra height amongst the left heights of L1 to L5 vertebrae in that case. Similarly, $max(H_c)$ and $max(H_r)$ are defined for the center and right heights. These deviation features are inspired from the radialogist's reports which quantify the compression of a fractured vertebra by comparing with a normal vertebra.

3.6.2 Classifiers

We experiment on a total of 15 cases for our automatic fracture detection out of which 7 cases have one or more than one lumbar vertebrae with wedge/compression fracture. We did not use all the 50 cases for classification since that would cause an imbalance in training data due to very few number of vertebrae with the kind of fracture we are trying to diagnose automatically. After the relevant features are extracted from each vertebra, we build five individual classfiers using existing modeling methods. The first classifier is an SVM (Support Vector Machine),[17] implemented using a polynomial kernel of degree 3. The second one is a kNN (k Nearest Neighbor) classifier, where k has been empirically fixed to 3. The third and fourth ones use LDA (Linear Discriminant Analysis) and QDA (Quadratic Discriminant Analysis) as classifiers respectively while the last one is a Naive Bayes classifier. Finally, we construct a majority voting classifier and discuss the results in the following sections.

4. EXPERIMENTS AND RESULTS

4.1 Segmentation

We validate our segmentation algorithm with 50 clinical CT volumes which are divided into 5 sets each having 10 cases. We evaluate the performance of our algorithm using two metrics:

1) The modified Hausdorff distance (average deviation of the contour):[18]

$$h(R,G) = (\sum_{i=1}^{|R|} min[\|R_i, G\|])/|R| \tag{5}$$

where $G \in$ Gold standard contour pixels and $R \in$ automatic segmentation contour pixels and $|R|$ denotes the total number of pixels in the automatic contour.

2) Over-segmentation (false positive rate) and under-segmentation (false negative rate),[14] are defined as follows, respectively:

$$O(S_r|S_g) = (|O|/|S_g|) * 100 \quad where \quad O = \{p|p \in S_r \quad and \quad p \notin S_g\} \tag{6}$$

$$U(S_r|S_g) = (|U|/|S_g|) * 100 \quad where \quad U = \{p|p \in S_g \quad and \quad p \notin S_r\} \tag{7}$$

where S_r and S_g are the pixels in the segmented region by automation and by hand (gold standard), respectively. For generation of the gold standard, we average the manually drawn contours from three experts (one radiologist and two trained students).

Table 1: Hausdorff distance in mm for 50 cases (10 cases each set).

Set	L1	L2	L3	L4	L5	Avg (mm)
1	1.2	1.2	1.2	1.2	1.4	1.2
2	1.3	1.5	1.5	1.5	1.8	1.5
3	1.5	1.2	1.4	1.6	1.8	1.5
4	1.0	1.1	1.4	1.4	1.4	1.3
5	1.0	1.0	1.0	1.2	1.4	1.1
Avg	1.2	1.2	1.3	1.4	1.6	1.5

Table 2: Over-segmentation in percentage.[14]

Set	L1	L2	L3	L4	L5	Avg (%)
1	12.1	13.0	14.3	14.4	16.9	14.1
2	12.5	16.9	19.3	13.8	25.6	17.6
3	17.0	16.9	17.7	20.1	25.2	19.4
4	12.8	12.2	15.8	19.4	16.7	15.4
5	10.6	12.9	10.4	12.9	14.5	12.3
Avg	13.0	14.4	15.5	16.1	19.8	15.8

Table 3: Under-segmentation in percentage.[14]

Set	L1	L2	L3	L4	L5	Avg (%)
1	5.9	6.1	3.8	3.7	5.1	4.9
2	10.1	8.8	7.2	13.3	5.2	8.9
3	4.9	4.4	4.4	3.0	3.0	3.9
4	3.4	3.1	3.7	1.5	3.8	3.1
5	4.4	3.0	5.1	3.9	6.0	4.5
Avg	5.7	5.1	4.8	5.1	4.6	5.1

Performance results ie. the Hausdorff distance, over-segmentation and under-segmentation are displayed in Tables 1, 2 and 3 respectively.

4.2 Classification

We experiment on 15 CT cases which have corresponding ground truth in the form of a radiologist's report. Here a positive class indicates presence of wedge/compression fracture while a negative class means absence of such fracture.

The performance metrics, specificity and sensitivity are defined as follows :

$$\text{Specificity} = \frac{\text{TNs}}{\text{TNs} + \text{FPs}} \quad \text{and} \quad \text{Sensitivity} = \frac{\text{TPs}}{\text{TPs} + \text{FNs}} \tag{8}$$

where TNs is the Number of True Negatives, FNs is the Number of False Negatives, TPs is the Number of True Positives. FPs is the Number of False Positives. The False Positive Rate(FPR) and the True Positive Rate(TPR), are defined as:

$$\text{FPR} = 1 - \text{Specificity} \quad \text{and} \quad \text{TPR} = \text{Sensitivity} \tag{9}$$

5. DISCUSSION

5.1 Segmentation

From Table 1 we observe that the Hausdorff distance (contour deviation from the gold standard) is the maximum for L5 vertebra with an average of $1.6mm$ while the average deviation for both L1 and L2 is $1.2mm$. Also the overall average is observed to be $1.5mm$. From Tables 2 and 3 we see that the over-segmentation(15.8%) is much higher than the under-segmentaton(5.1%). Moreover, over-segmentation rates are in the range of 14% - 26% for the L5 vertebrae and could be improved.

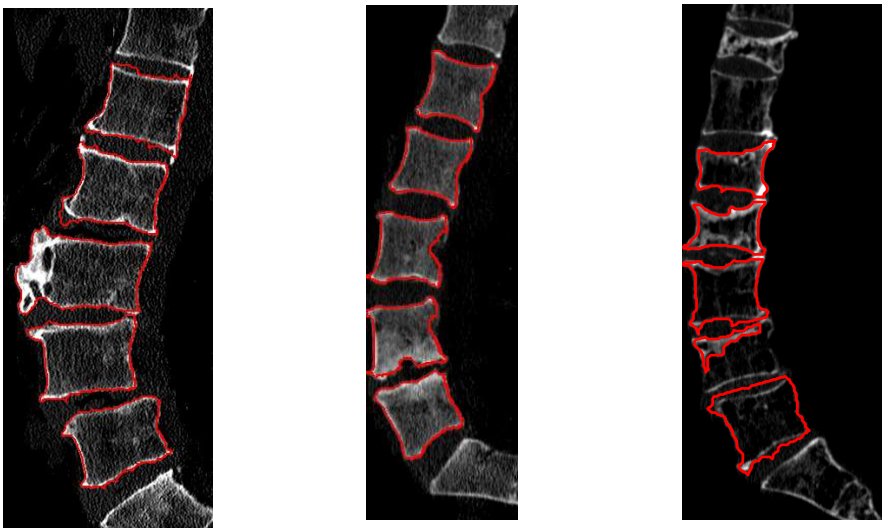

(a) (b) (c)

Figure 4: Some sample automatic segmentation results : (a) and (b) shows 2 samples of successful segmentation of L1 to L5 vertebrae , (c) shows a sample of an unsuccessful segmentation where L1,L2,L3 and L5 are successful but L4 fails.

Figure 4 shows a few sample segmentation results of our automatic algorithm. While 4(a) and 4(b) shows 2 cases where segmentation of all the five lumbar vertebra is successful, 4(c) shows a case where L4 segmentation fails completely due to very low pixel intensities.

Table 4: Classifier performance results in percentage for 15-fold cross validation

Classifier	**Accuracy**	**Specificity**	**Sensitivity**
SVM	94.667	96.825	83.333
3NN	94.667	100	66.667
LDA	94.667	98.413	75.0
QDA	97.333	98.413	91.667
Naive Bayes	96.0	96.825	91.667
Majority Vote (SVM+QDA+NaiveBayes)	97.333	98.413	91.667

5.2 Classification

We perform 15-fold cross-validation experiments on each of our classifiers and observe that while the all the classifiers show a high accuracy, the kNN and LDA classfiers have a low sensitivity *i.e.* a low true positive rate (Table 4). Hence, we construct a majority voting classifier, by combining the results from three of our classifiers : SVM, QDA and Naive Bayes and selecting the label given by two or more classifiers as the final result. Majority voting not only guarantees better performance than the worst individual classifier, it also avoids classifier evaluation steps used in complex fusion algorithms. It has also been shown experimentally[19] and mathematically[20] that a majority voting classifier can show improvement over individual classifier accuracy. The performance results of all our classifiers are shown in Table 4. The accuracy values indicate that the feature selection for classification is fairly good and that quadratic classifiers perform better than the linear ones due to the nature of our data. Further, QDA and the majority vote classifier show a high accuracy 97.33%, along with a high sensitivity (True Positive Rate) of 91.67%.

6. CONCLUSION

We proposed a fully automated method for segmentation of lumbar vertebrae from clinical CT volumes based on geometry and intensity features. Initially, we localize and label the intervertebral discs using a two-level probabilistic model using both pixel-level (intensity) and object-level (location) features. Then we segment a rough Region of Interest (ROI) of the vertebral body using a series of morphological operations. After that we detect angle-constrained Hough lines for each disc level from the gradient image and average their slopes to calculate the lines separating the five lumbar vertebrae. Finally we segment the individual lumbar vertebrae by morphological and hole-filling operations. Our segmentation shows an average contour deviation of $1.5mm$ on 50 CT cases which contain various types of fractures, bone spurs and many disc abnormalities. We have also presented the step by step preparation of the segmented vertebrae to provide suitable height related features to detect wedge compression fractures with an accuracy of 97.3% and sensitivity of 91.67%. A high sensitivity (or high true positive rate) is very essential for any lumbar diagnosis system. This is because, while a high false positive rate can be quickly rectified by the radiologist, a low true positive rate might lead to a fractured vertebra not being diagnosed at all, and hence a greater penalty. Thus we have designed a fully automatic, high accuracy and high sensitivity computer-aided system for lumbar compression fracture diagnosis. Implementation of such systems in large-scale facilities will not only reduce the burden on a radiologist, but will also boost confidence on a diagnosis. Occasionally, a robust CAD system, might also detect a disorder that a radiologist could have missed due to insufficient time to analyze a case. Currently we have experimented with a total of 15 clinical CT cases for the automatic diagnosis out of which 7 cases have one or more wedge compression fractures. We did not use all the 50 CT cases due to the low number of cases with compression fracture. In the near future we aim to collect more CT cases with the relevant type of fracture, so that we can model our classifiers accurately and build robust CAD systems. We will also extend our work to clinical MRI cases to detect fractures and diagnose pathological conditions like osteoporosis and malignancies. In today's world, there are numerous lumbar disorders affecting a vast number of people thoughout the planet; hence the future holds a large scope for autonomous automatic diagnostic systems.

7. ACKNOWLEDGEMENT

The authors would like to thank Ruchika Mehresh (Phd Student, CSE, UB) for her help with the manual segmentation of the lumbar CT scans.

REFERENCES

[1] NINDS, "National institute of neurological disorders and stroke : Low back pain fact sheet," (2008).
[2] Andrew L Sherman and Nizam Razack, "Lumbar compression fracture," *eMedicine* (2010). Online article.
[3] D. H. Kim, A. R. Vaccaro, "Osteoporotic compression fractures of the spine; current options and considerations for treatment," *The spine journal : official journal of the North American Spine Society* (2006).
[4] WHO, "Assessment of fracture risk and its application to screening for postmenopausal osteoporosis. report of a who study group," *World Health Organization technical report series* (1994).
[5] M. G. Roberts, T. F. Cootes, J. Adams, "Segmentation of lumbar vertebrae using part-based graphs and active appearance models," in [*MICCAI '09: Proceedings of the 12th international conference on Medical Image Computing and Computer-Assisted Intervention - Part II*], 1017–1024 (2009).
[6] A. Mastmeyer, K. Engelke, C. Fuchs, W. Kalender, "A hierarchical 3d segmentation method and the definition of vertebral body coordinate systems for qct of the lumbar spine," *Medical Image Analysis* **10**, 560 – 577 (2006).
[7] S. Schmidt, J. Kappes, M. Bergtholdt, V. Pekar, S. Dries, D. Bystrov, C. Schnoerr, "Spine detection and labeling using a parts-based graphical model," in [*IPMI'07: Proceedings of the 20th international conference on Information processing in medical imaging*], 122–133 (2007).
[8] R. S. Alomari, J. J. Corso, V. Chaudhary, "Labeling of lumbar discs using both pixel- and object-level features with a two-level probabilistic model," *IEEE Transactions on Medical Imaging* **29**. in press.
[9] R. S. Alomari, J. J. Corso, V. Chaudhary, G. Dhillon, "Desiccation diagnosis in lumbar discs from clinical mri with a probabilistic model," in [*In the proceedings of the IEEE International Symposium on Biomedical Imaging (ISBI09)*], 546–549 (June 28 2009).
[10] R. S. Alomari, J. J. Corso, V. Chaudhary, G. Dhillon, "Computer-aided diagnosis of lumbar disc pathology from clinical lower spine mri," *International Journal of Computer Aided Radiology and Surgery* **5**, 287–293 (May 2010).
[11] R. S. Alomari, J. J. Corso, V. Chaudhary, G. Dhillon, "Automatic diagnosis of lumbar disc herniation using shape and appearance features from mri," in [*In the proceedings of SPIE medical imaging, computer aided diagnosis (CAD)*], (2010).
[12] J. Kaminsky, P. Klinge, T. Rodt, M. Bokemeyer, W. Luedmann, M. Samii, "Specially adapted interactive tools for an improved 3d-segmentation of the spine," *Computerized Medical Imaging and Graphics* **28**, 119 – 127 (2004).
[13] B. Naegel, "Using mathematical morphology for the anatomical labeling of vertebrae from 3d ct-scan images," *Computerized Medical Imaging and Graphics* **31**, 141 – 156 (2007).
[14] H. Shen, A. Litvin, C. Alvino, "Localized priors for the precise segmentation of individual vertebras from ct volume data," in [*MICCAI '08: Proceedings of the 11th international conference on Medical Image Computing and Computer-Assisted Intervention - Part I*], **11**, 367–375 (2008).
[15] T. Klinder, J. Ostermann, M. Ehm, A. Franz, R. Kneser, C. Lorenz, "Automated model-based vertebra detection, identification, and segmentation in ct images," *Medical Image Analysis* **13**, 471–482 (2009).
[16] G. N. Hounsfield, "Nobel award address. computed medical imaging," *Medical Physics* **7**, 283–290 (Jul-Aug 1980).
[17] C. Cortes, V. Vapnik, "Support-vector networks," *Machine Learning* **20**, 273–297 (1995).
[18] S. Kompalli, M. Alam, R. S. Alomari, S. T. Lau, V. Chaudhary, "Design of a benchmark dataset, similarity metrics, and tools for liver segmentation," in [*Society of Photo-Optical Instrumentation Engineers (SPIE) Conference Series*], (2008).
[19] Muhammad A. Khany, Zahoor Jan, Anwar M. Mirzaz, "Performance analysis of classifier fusion model with minimum feature subset and rotation of the dataset," in [*Proc. of 6th international conference on Fuzzy systems and knowledge discovery*], 251–255 (2009).
[20] L. I. Kuncheva, C. J. Whitaker, R. P. W. Duin, "Limits on the majority vote accuracy in classifier fusion," *Pattern Analysis and Applications* **6**, 22–31 (2003).